

Reactivity of gaseous PtO₂ and RhO₂ with LaNiO₃ thin films; a systematic XPS study

J. Hessevik*^a, H. H. Sønsteby^a, H. Fjellvåg^a, A. O. Sjøstad*^a

^a Department of Chemistry, Centre for Materials Science and Nanotechnology, University of Oslo, N-0318 Oslo, Norway.

Section S1. Supplementary figures and text to experimental part and to results part 3.1 on reference samples

Experimental details on thermogravimetric determination of formula weight of Ni acetate and Rh nitrate hydrate:

For Ni acetate: Small porcelain crucibles were heated to 800 °C overnight and cooled in a desiccator. Around 2.5 g of Ni acetate was added gravimetrically. Glass wool was added followed by a repeated weighing. The crucibles were heated in air at 800 °C for 3 days and cooled in a desiccator. This procedure assured quantitative conversion into NiO. From the weight changes, the formula weights of the acetate was calculated. Four parallel determinations were carried out.

For Rh nitrate hydrate: Thermogravimetric analysis of Rh nitrate hydrate (Fig. S1) was performed with a NETZSCH TG 209F1 Libra instrument operated with alumina crucibles, 50 vol. % O₂ in N₂ gas mixture at a flow of 40 mL/min and heated with heating rate of 5 °C/min up to 850 °C. The formula mass of Rh nitrate hydrate could be calculated from the measured mass loss due to full conversion to Rh₂O₃.

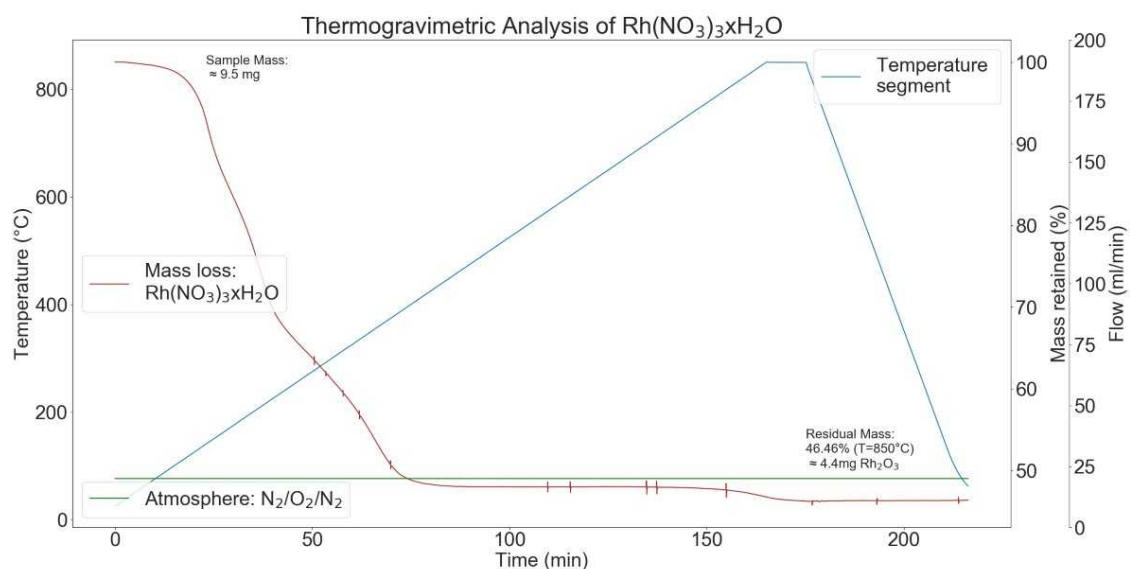


Fig. S1 Thermogravimetric analysis of Rh nitrate hydrate in 50 vol.% O₂ in N₂ gas mixture at a flow of 40 mL/min and heating rate of 5 °C/min.

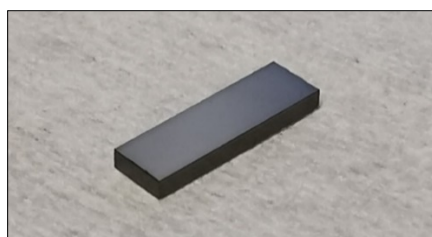


Fig. S2 LNO thin film on STO substrate.

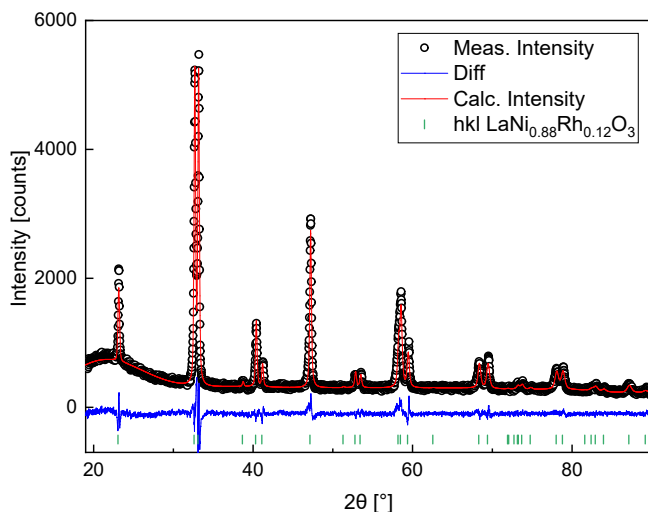


Fig. S3 Rietveld refinement of powder x-ray diffractogram of synthesized powder of $\text{LaNi}_{0.88}\text{Rh}_{0.12}\text{O}_3$ show a phase pure rhombohedral (R-3c) structure.

Section S2. Fitting of XPS data for reference samples (powders of $\text{La}_2\text{NiPtO}_6$, $\text{LaNi}_{0.95}\text{Pt}_{0.05}\text{O}_3$, $\text{LaNi}_{0.88}\text{Rh}_{0.12}\text{O}_3$ and LaRhO_3)

The reference samples were measured without electrical contact and they had to be calibrated to the C1s signal of adventitious carbon contamination. Narrow scans of C1s were fitted with four single peaks: C-(C,H), C-(O,N), C=O and O=C-O. The C-(C,H) peak was calibrated to be 284.8 eV. The BE of the C-(O,N) peak was fixed to the BE of C-(C,H) peak + 1.50 (± 0.1) eV, while BE of C=O was fixed to the BE of O=C-O peak + 3.20 (± 0.2) eV, and let the last peak of O=C-O peak BE refine freely ([1]). An example fit is shown for the $\text{La}_2\text{NiPtO}_6$ reference sample in Fig. S4, where the C1s peak for C-(C,H) is fitted to be 282.52 eV. Relative to a reference on 284.8 eV, a correction of Pt4f peaks in $\text{La}_2\text{NiPtO}_6$ +2.28 eV is needed. A similar procedure was used to also find the correction values for $\text{LaNi}_{0.95}\text{Pt}_{0.05}\text{O}_3$ (+2.93 eV), $\text{LaNi}_{0.88}\text{Rh}_{0.12}\text{O}_3$ (+3.25 eV) and LaRhO_3 (+2.56 eV).

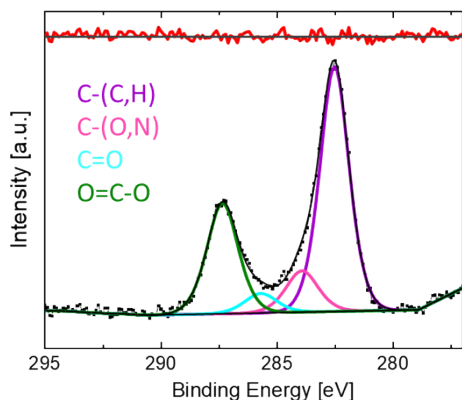


Fig. S4 Peak fitting in XPS of C1s peaks, C-(C,H), C-(O,N), C=O and O=C-O, from adventitious carbon contamination on the surface of $\text{La}_2\text{NiPtO}_6$ reference sample

Narrow scans of Pt4f for $\text{La}_2\text{NiPtO}_6$ reference sample (Fig. S5) were fitted with one doublet of Pt4f (with spin orbit splitting (SOS) = 3.3 ± 0.2 eV, height ratio of $\text{Pt}4f_{7/2}$ to $\text{Pt}4f_{5/2}$ = 0.75, L/G-mix refined to 70 % from a starting point of 50 %, slightly asymmetric peaks were allowed by refining tail mix and tail exponent at the same time, FWHM refined to 1.16 eV) and three sets of Ni3p doublets due to the presence of both Ni^{3+} , Ni^{2+} and shake up peaks (the L-G mix was fixed to 50 % for the Ni peaks, SOS of $\text{Ni} 3p_{3/2}$ and $\text{Ni} 3p_{1/2}$ were fixed to 2.2 ± 0.2 eV, height ratios of the $\text{Ni}3p_{1/2}$ to $\text{Ni}3p_{3/2}$ was fixed to 0.5 eV, the FWHM of Ni^{3+} was refined to 3.1 eV from a starting guess of 3.3 eV and the FWHM of Ni^{2+} was refined to 2.5 eV from a starting guess of 2.7 eV, the binding energies (BEs) of $\text{Ni}3p_{3/2}$ of Ni^{2+} and Ni^{3+} were fixed to 64.91 eV (+2.28 eV = 67.19 eV) and 69.20 eV (+2.28 eV = 71.48 eV), a doublet of Ni was added to represent satellite/shake-up peaks that overlaps with the Pt4f peaks, but are just

briefly approximated here with the height of the $\text{Ni}3p_{3/2}$ being fixed with the same ratio to $\text{Ni}3p_{3/2}$ peak of Ni^{2+} peak in a pristine LNO thin film. The parameters chosen above build on results from fitting $\text{Ni}3p$ peaks of a pristine LNO thin film, as described later for Fig. S19 in section S4. The BE of $\text{Pt}4f_{7/2}$ ended at 71.87 eV, however, after correction to C1s it has a BE of 74.15 eV.

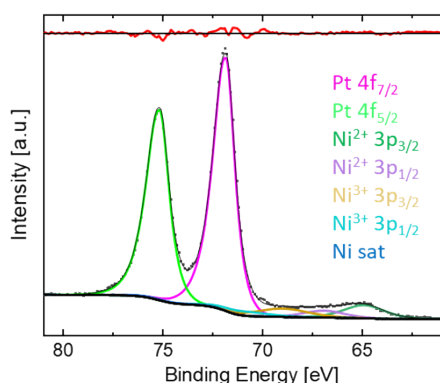


Fig. S5 Peak fitting of XPS data from $\text{La}_2\text{NiPtO}_6$ reference sample with peaks of Pt4f, Ni^{2+} , Ni^{3+} and Ni satellite or shakeup peaks. Not corrected against C1s in figure.

Narrow scans of Pt4d for the $\text{La}_2\text{NiPtO}_6$ reference sample (Fig. S6) were fitted with one set of Pt4d doublet with $\text{SOS} = 17.0 \pm 0.2$ eV, height ratio between $\text{Pt}4d_{3/2}$ and $\text{Pt}4d_{5/2}$ fixed to 0.67, FWHM ended at 4.25, L-G mix refined to about 87 % and asymmetric peak shapes by refining peak tail mix and tail exponent. Two peaks appear at higher BEs and could be satellite/shake-up peaks of Pt4d. Peak BE of $\text{Pt}4d_{5/2} = 314.87$ eV, and with a correction of +2.28, it ends up at 317.14 eV.

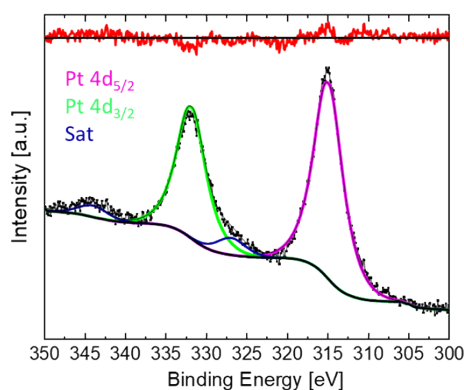


Fig. S6 Peak fitting of XPS data from $\text{La}_2\text{NiPtO}_6$ reference sample with peaks of Pt4d and one unknown peak. Not corrected against C1s in figure.

Narrow scans of Pt4f for $\text{LaNi}_{0.95}\text{Pt}_{0.05}\text{O}_3$ reference sample (Fig. S7) was fitted in the same way as for the $\text{La}_2\text{NiPtO}_6$ reference sample. The FWHM of $\text{Pt}4f_{7/2}$ ended at 0.81 eV, L-G mix of 99 % and the peaks show asymmetry, which could fit well with $\text{LaNi}_{0.95}\text{Pt}_{0.05}\text{O}_3$ having metallic character. The Ni3p peaks are not fitted as well for this sample, however, BEs of platinum signals are expected to not be too affected by that since the peak position of $\text{Pt}4f_{7/2}$ is restricted to a SOS of $3.3 (\pm 0.2)$ eV relative to the $\text{Pt}4f_{5/2}$. The BE of $\text{Pt}4f_{7/2}$ was fitted to 70.34 eV, and with a correction of 2.93 eV, it ends up at 73.27 eV.

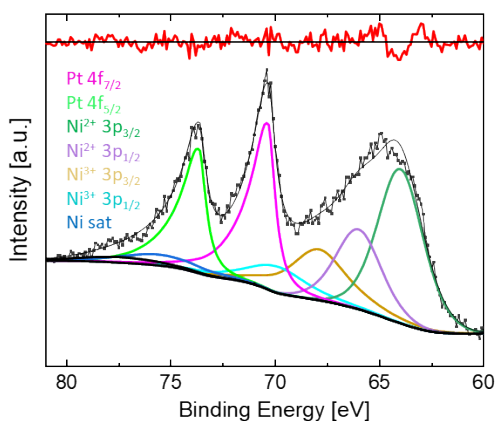


Fig. S7 Peak fitting of XPS data from $\text{LaNi}_{0.95}\text{Pt}_{0.05}\text{O}_3$ reference sample with peaks of Pt4f, Ni^{2+} , Ni^{3+} and Ni satellite or shakeup peaks. Not corrected against C1s in figure.

Narrow scans of Pt4d for the $\text{LaNi}_{0.95}\text{Pt}_{0.05}\text{O}_3$ reference sample (Fig. S8) have a low signal-to-noise ratio and the data quality is too low for proper peak fitting. Two extra peaks at higher binding energies (above 340 eV) can be tiny impurities of Ca in the sample.

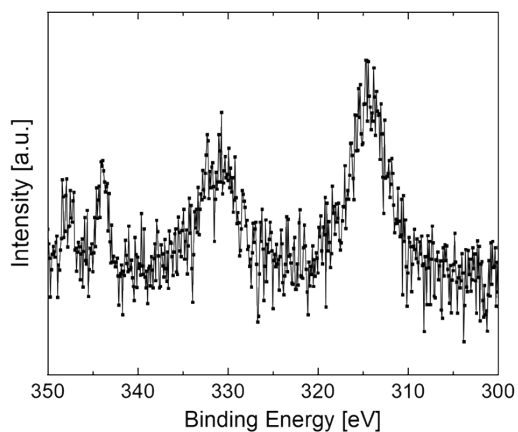


Fig. S8 XPS data from $\text{LaNi}_{0.95}\text{Pt}_{0.05}\text{O}_3$ reference sample with peaks of Pt4d and Ca2p impurities. Not corrected against C1s in figure.

Narrow scans of Rh3d for LaRhO_3 reference sample (Fig. S9) was fitted with two doublets of Rh3d peaks with SOS fixed to 4.71 ± 0.2 eV. FWHM of $\text{Rh}3d_{3/2}$ was allowed to be broader than $\text{Rh}3d_{5/2}$ due to the possible Coster-Konig effect and area ratio between $\text{Rh}3d_{3/2}$ and $\text{Rh}3d_{5/2}$ was fixed to the theoretical value of 0.67. The L-G mix was refined to 75 % and 65 % for the peaks corresponding to Rh(IV) and Rh(III) from a starting guess of 50 %, respectively. The BEs of $\text{Rh}3d_{5/2}$ were fitted to 305.81 eV and 306.96 eV, and after correction with +2.56, they end up at 308.4 eV and 309.5 eV.

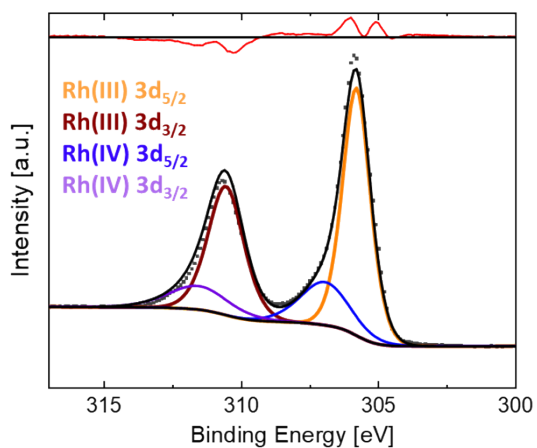


Fig. S9 Peak fitting of XPS data from LaRhO_3 reference sample with peaks of Rh3d.

Narrow scans of Rh3d for $\text{LaNi}_{0.88}\text{Rh}_{0.12}\text{O}_3$ reference sample (Fig. S10) was fit with two doublets of Rh3d peaks with SOS fixed to 4.71 ± 0.2 eV. FWHM of $\text{Rh}3d_{3/2}$ was allowed to be broader than $\text{Rh}3d_{5/2}$ due to the possible Coster-Konig effect and area ratio between $\text{Rh}3d_{3/2}$ and $\text{Rh}3d_{5/2}$ was fixed to the theoretical value of 0.67. The L-G mix was fixed to 80 % and asymmetric peak shape allowed for Rh(III) due to assumed metallic character in rhombohedral $\text{LaNi}_{0.88}\text{Rh}_{0.12}\text{O}_3$. The BEs of $\text{Rh}3d_{5/2}$ were fitted to 304.77 eV and 306.29 eV, and after correction with +3.25 eV, they end up at 308.0 eV and 309.5 eV. Depending on how large the tail of Rh(III) is compared to how much Rh(IV) is there, the BE of Rh(III) is not changed but BE of $\text{Rh}3d_{5/2}$ of Rh(IV) is varying from 309.1-309.5 eV.

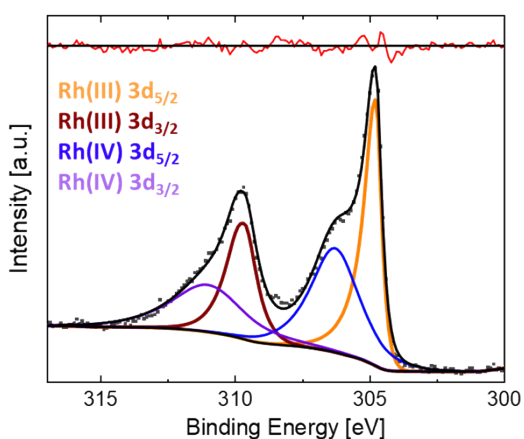


Fig. S10 Peak fitting of XPS data from $\text{LaNi}_{0.88}\text{Rh}_{0.12}\text{O}_3$ reference sample with peaks of Rh3d.

Section S3. Supplementary figures to results part 3.2

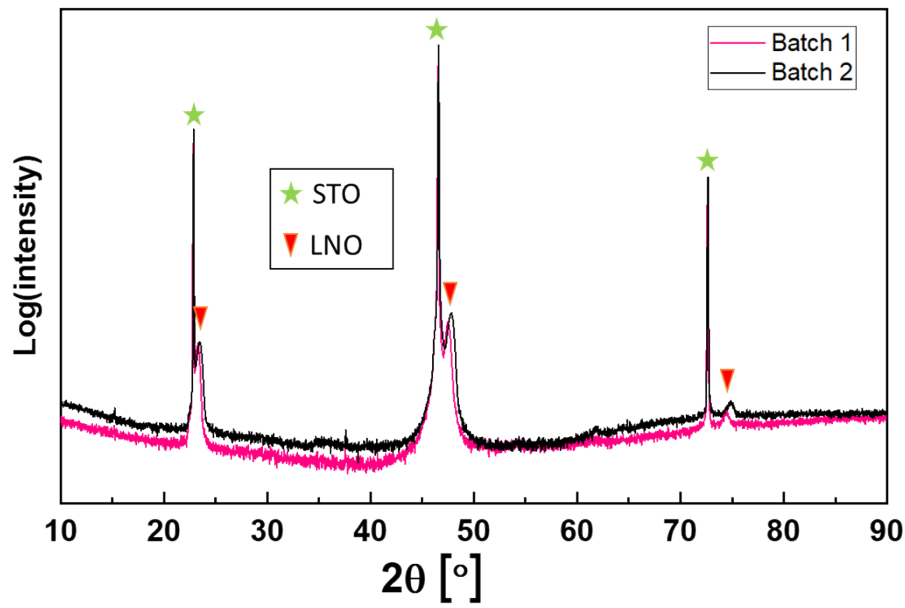


Fig. S11 Powder X-ray diffractograms of pristine LNO thin film onto STO substrate. (h00) peaks for STO are at a few degrees lower than pseudo cubic (h00) peaks for LNO.

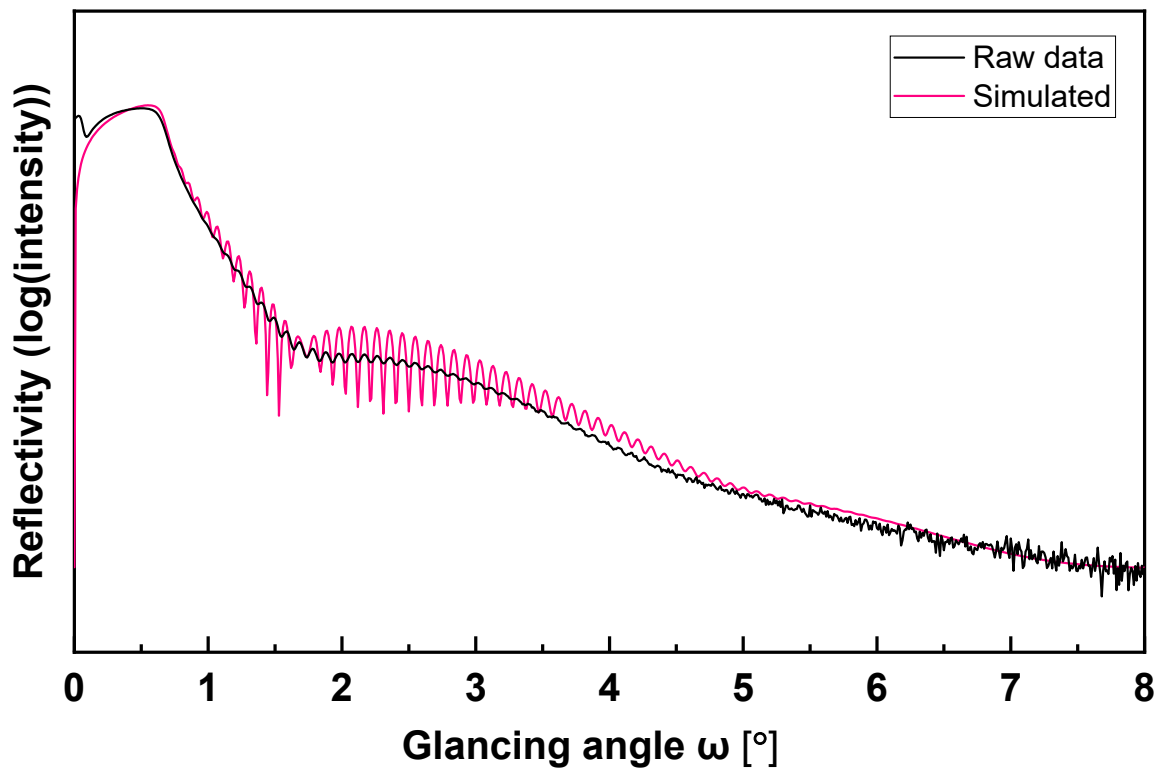


Fig. S12 X-ray reflectometry (XRR) raw data of batch 1 fitted to a periodicity which resembles thickness of film of 88.2 nm.

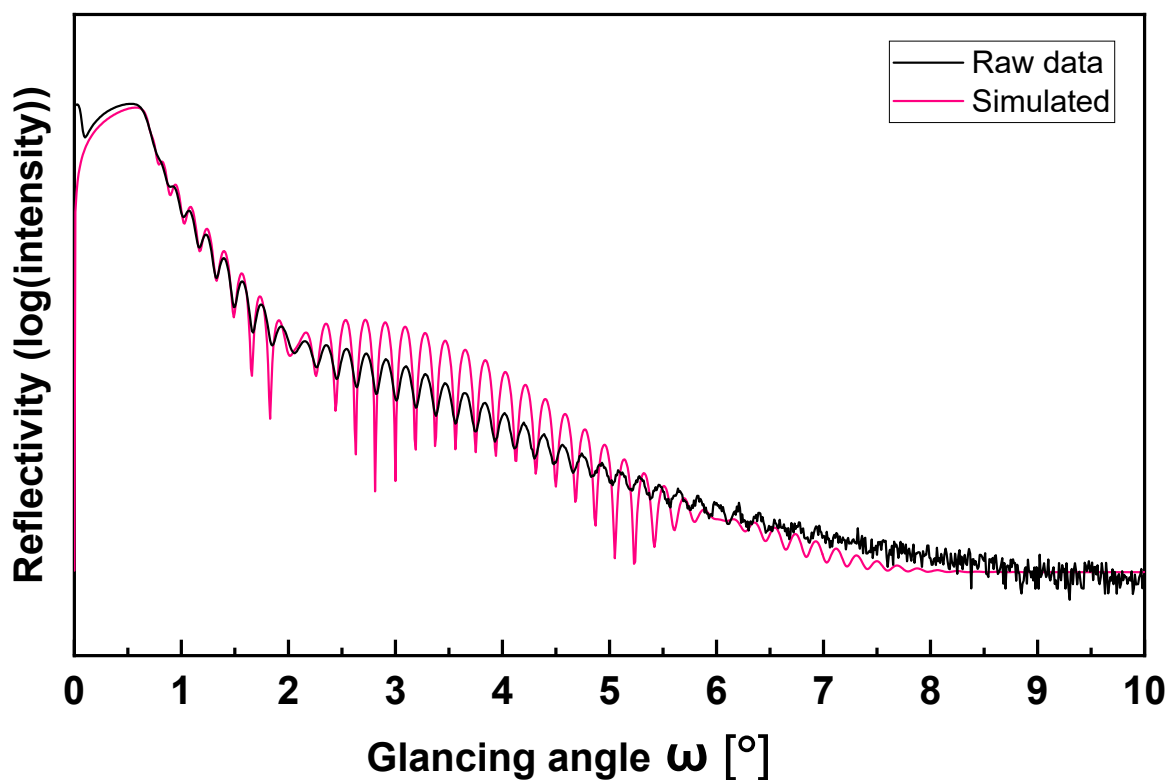


Fig. S13 X-ray reflectometry (XRR) raw data of batch 2 fitted to a periodicity which resembles thickness of film of 45.3 nm.

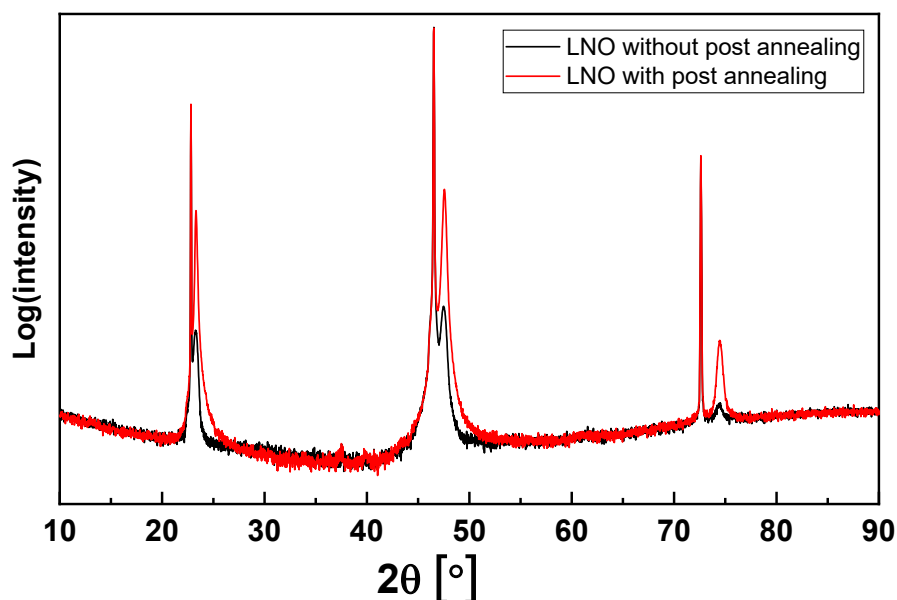


Fig. S14 Powder X-ray diffractograms of “as-grown” LNO thin film without post deposition annealing and post annealed LNO thin film onto STO substrate. (h00) peaks for STO are at a few degrees lower than pseudo cubic (h00) peaks for LNO.

Survey spectra of pristine LNO before and after Ar^+ sputtering (Fig. S15) illustrate why only platinum and rhodium concentration depth profiles after Ar^+ sputtering are given, and why only BEs of Pt/Rh peaks and not concentrations at the surface (before Ar^+ sputtering) are examined and shown in the following sections.

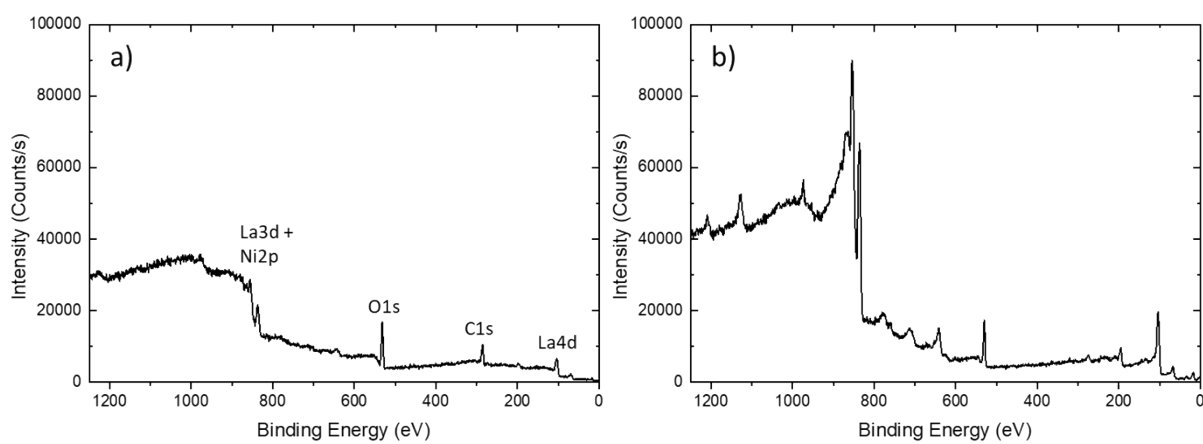


Fig. S15 XPS survey spectra of pristine LNO thin film (Batch 1) a) at the surface and b) after 26 seconds Ar⁺ sputtering.

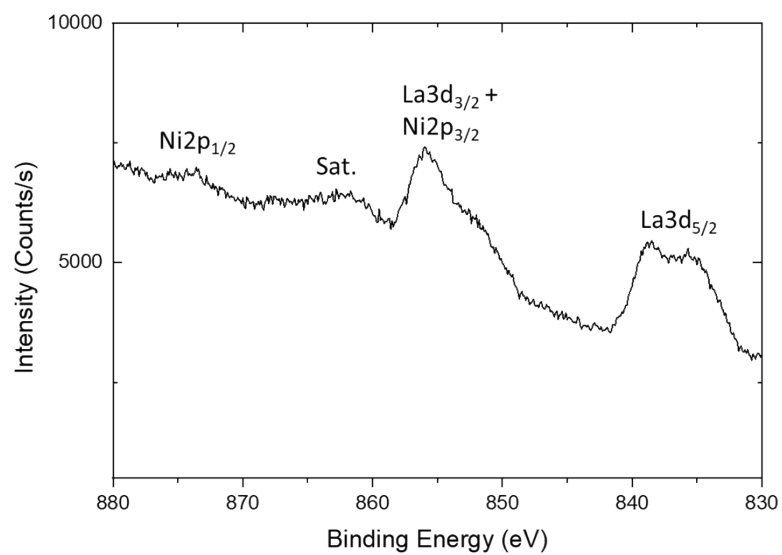


Fig. S16 XPS narrow scan of surface of pristine LNO thin film (Batch 1) showing overlapping La3d and Ni2p peaks.

Section S4. Supplementary figures to results section 3.3 and fitting of XPS data

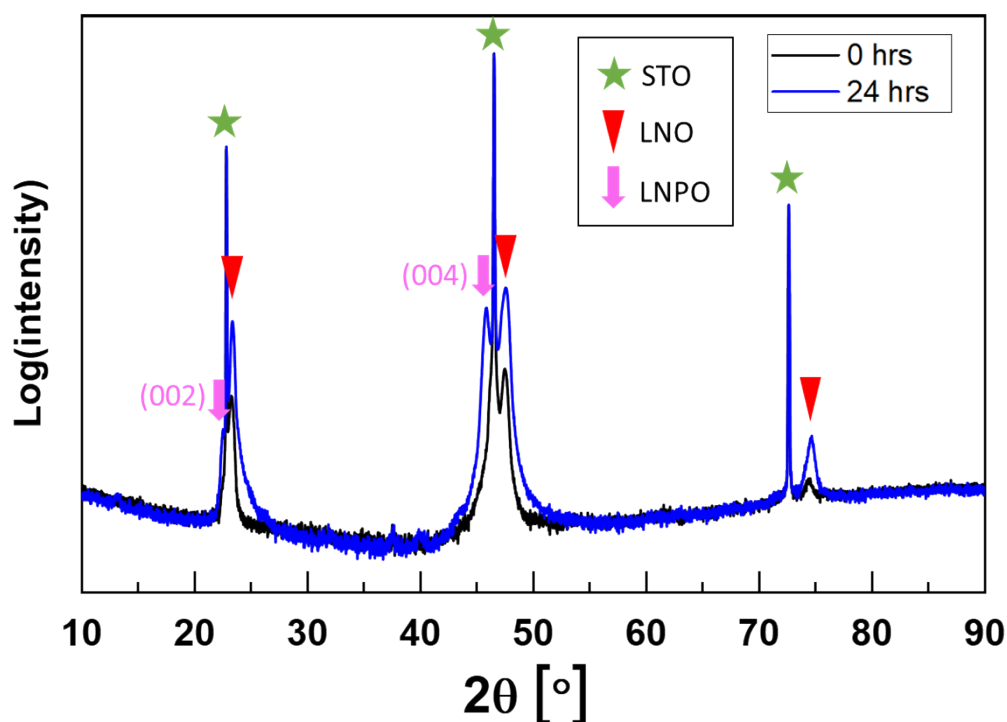


Fig. S17 Powder X-ray diffractograms of “as-grown” LNO thin film without post deposition annealing and after 24 hrs $\text{PtO}_2(\text{g})$ exposure. STO = SrTiO_3 , LNO = LaNiO_3 and LNPO = $\text{La}_2\text{Ni}_{2-2x}\text{Pt}_{2x}\text{O}_6$ ($0.2 \leq x \leq 0.5$).

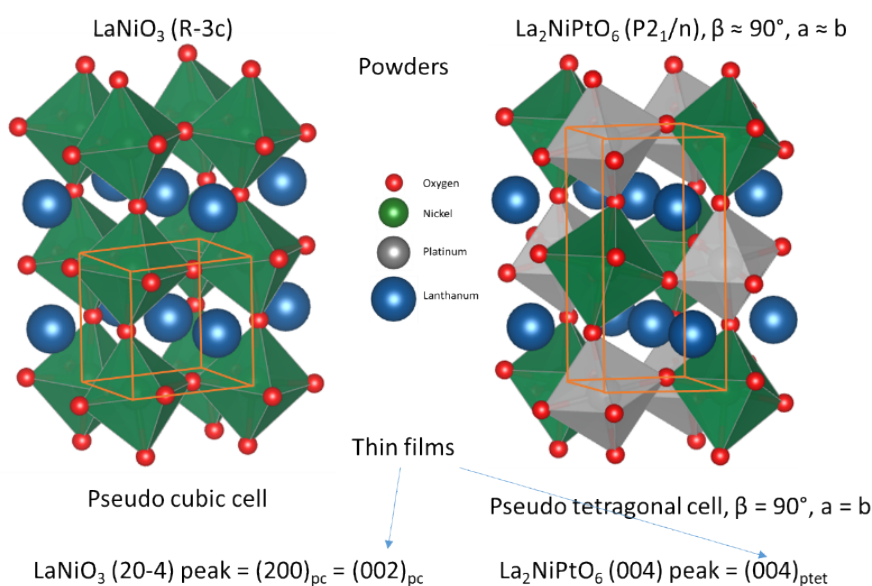


Fig. S18 Crystal structure of LNO and $\text{La}_2\text{NiPtO}_6$ showing the pseudo cubic cell and pseudo tetragonal (ptet) cell of thin films grown epitaxially on STO substrates.

XPS fitting of $\text{Ni}3\text{p}$ peaks of LNO thin films from batch 1 is shown in Fig. S19. For the pristine LNO thin film (a), the spin orbit splitting (SOS) of $\text{Ni}3\text{p}_{3/2}$ and $\text{Ni}3\text{p}_{1/2}$ were fixed to 2.2 ± 0.2 eV, height ratios of the $\text{Ni}3\text{p}_{1/2}$ to $\text{Ni}3\text{p}_{3/2}$ was fixed to 0.5 eV, the FWHM of Ni^{3+} was fixed to 3.3 ± 0.1 eV and the FWHM of Ni^{2+} was fixed to 2.7 ± 0.1 eV, the starting guesses of binding energies (BEs) of $\text{Ni}3\text{p}_{3/2}$ of Ni^{2+} and Ni^{3+} were set to 66.9 and 71.0 and let to refine with a restriction of BE (Ni^{3+}) being 4.0 ± 0.2 eV of BE (Ni^{2+}) [2], and since pseudo-voigt functions (as a product of Lorentzian and Gaussian functions) were used in Thermo Avantage software, a L/G-mix of 50 % was used for Ni^{2+} as that probably has compound characteristics and a L/G-mix of 80 % was used for Ni^{3+} as that probably has

metallic characteristics similar to LaNiO_3 [3]. Some peaks at high BEs were not well fitted, and so a doublet of Ni was added with FWHM fixed to 5.0 ± 0.1 eV. This might be satellite or shake-up peaks, however, due to little information of these in literature, they are just briefly approximated here. After sputtering the LNO thin film, these peaks seem more pronounced. The same settings were used when fitting the LNO thin film after Ar^+ sputtering (b), however, an additional doublet of Ni3p peaks were added due to assumed reduction of oxidic nickel to nickel metal. BEs of the $\text{Ni}3p_{3/2}$ was fixed to 66.2 eV based on literature values for metallic Ni [4], and the best fit seemed to be with FWHM of 1.7 ± 0.1 eV. Interestingly, Ni^{3+} and Ni^{2+} seem to still be represented in the film after Ar^+ sputtering. It could maybe be expected that at least Ni^{3+} should have reduced completely to Ni^{2+} . Since the data is a bit noisy, it is difficult to conclude if the reduced species is Ni metal or if some Ni has just partly reduced.

It could be expected that Ni should be in oxidation state +3 in pristine LNO, however, the top surface of the thin film seems to have Ni both in oxidation state +2 and +3. This is supported by earlier reports, showing that oxygen vacancies are predominant in the surface layers of LaNiO_3 [5].

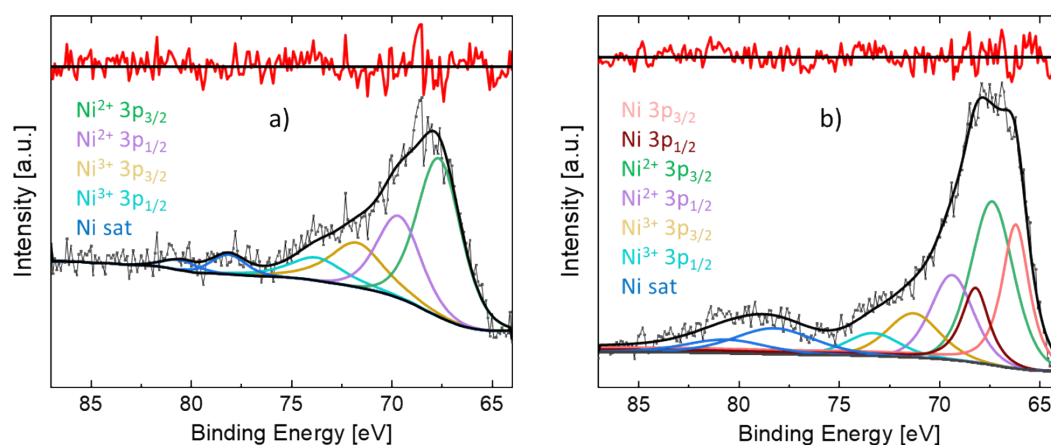


Fig. S19 XPS fitting of a) top surface of pristine LNO thin film from batch 1 and b) surface after 26 sec Ar^+ sputtering of same LNO film as in a).

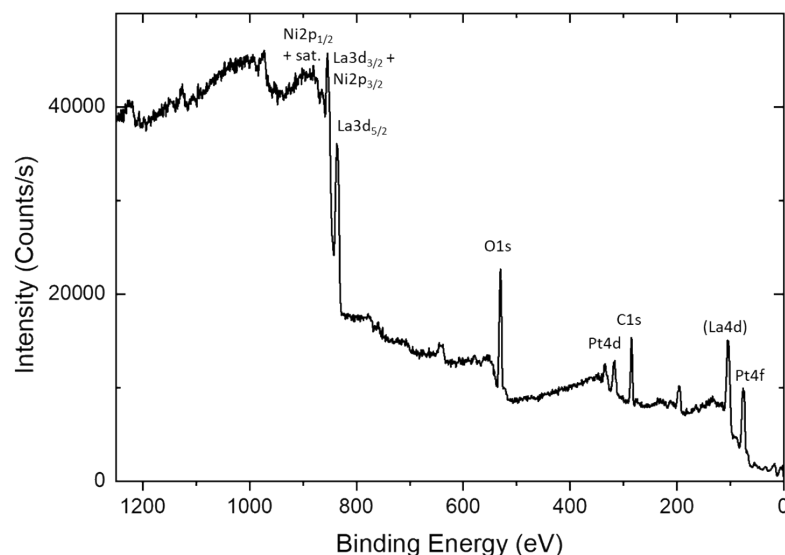


Fig. S20 XPS survey spectrum of LNO (Batch 1 without post annealing) after exposure to $\text{PtO}_2(\text{g})$ for 24 hrs with the most pronounced peaks identified.

XPS fitting of Pt4f and Ni3p peaks for LNO (without post deposition annealing) exposed to PtO_2 for 24 hrs, as shown in Fig. 3, included a doublet of Pt4f with SOS = 3.3 ± 0.2 eV, height ratio of $\text{Pt}4f_{7/2}$ to $\text{Pt}4f_{5/2}$ = 0.75, L/G-mix of 50 %, FWHM refined to 2.2 eV, while the Ni3p peaks were fitted similar to as shown in Fig. S19a) (except

that the height of the satellite/shakup peak was fixed to the same ratio it had in relation to the Ni²⁺ peak in Fig. S19a since it now overlapped with Pt4f_{5/2} and all L/G-mix values were fixed to 50%).

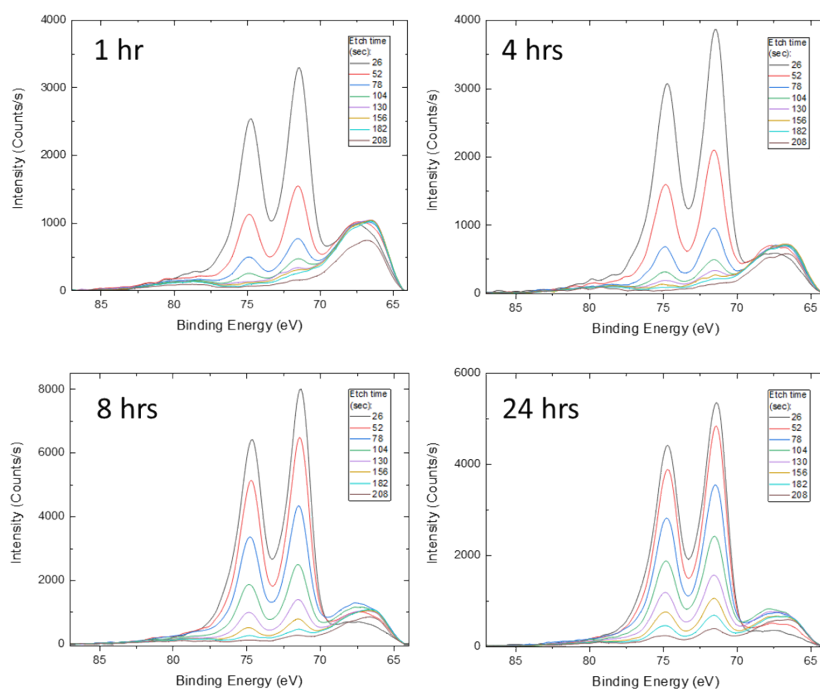


Fig. S21 XPS narrow scans of Pt4f (64-87 eV) at the different sputtering levels after sequential sputtering with Ar⁺ and measuring with XPS through the depth of the film for LNO (without post deposition annealing) after PtO₂ exposure for 1, 4, 8 and 24 hrs. For easier visualization, the data has been modified with a baseline removal (with a PCA reconstruct by finding factors of 6) and with Gaussian smoothing of FWHM of about 0.5 eV.

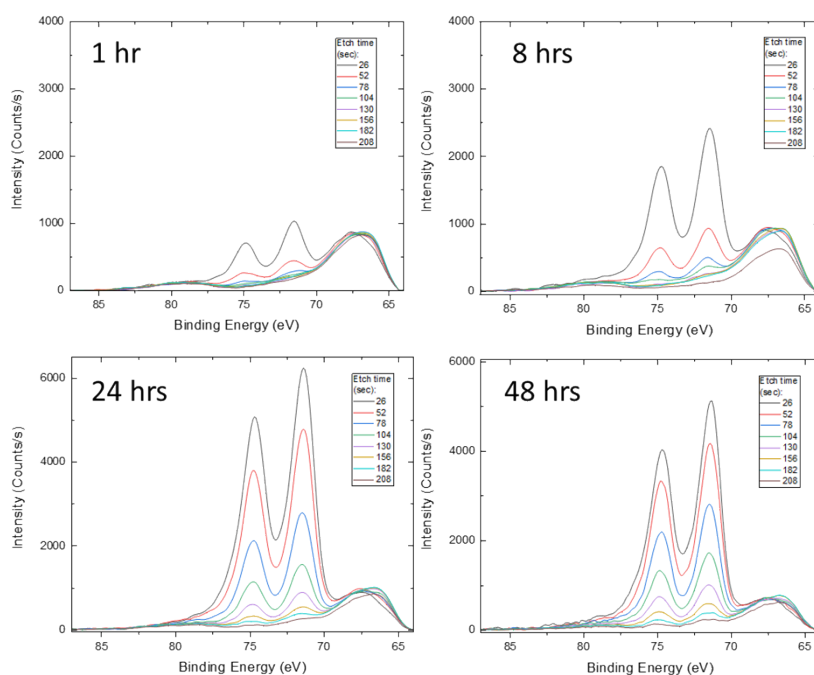


Fig. S22 XPS narrow scans of Pt4f (64-87 eV) at the different sputtering levels after sequential sputtering with Ar⁺ and measuring with XPS through the depth of the film for LNO (with post deposition annealing) after PtO₂ exposure for 1, 4, 8 and 24 hrs. For easier visualization, the data has been modified with a baseline removal (with a PCA reconstruct by finding factors of 6) and with Gaussian smoothing of FWHM of about 0.5 eV.

XPS fitting of Pt4f and Ni3p peaks for LNO (without post deposition annealing) exposed to PtO₂ for 24 hrs after 78 and 182 sec Ar⁺ sputtering is shown in Fig. S23. A doublet of Pt4f is included, with SOS = 3.3 ± 0.2 eV, height ratio of Pt4f_{7/2} to Pt4f_{5/2} = 0.75, L/G-mix of 50 %, FWHM fixed to 1.4 ± 0.1 eV and asymmetry allowance by refining tail mix and tail exponent at the same time. The Ni3p peaks were fitted similarly to as shown in Fig. S19b), except that the height of the satellite peak was fixed to the same ratio it had in relation to the Ni²⁺ peak in Fig. S19b since it now overlapped with Pt4f_{5/2} and all L/G-mix values were fixed to 50%. The fit is not perfect in the lower BE-region of the Ni 3p overlap area, possibly due to Ni only being partly reduced or it could be due to some uncertainties in the approximations of the line shapes. The fact that Ni might have different chemical shifts whether it is in NiO, La₂Ni_{2.2x}Pt_{2x}O₆ or LaNiO₃/oxygen deficient LaNiO_{3-x}, makes it even more difficult to interpret this region. Nevertheless, Ni3p peaks of Ni³⁺ are the ones that overlap the most with Pt4f. Small uncertainties in the quantifications of Pt4f arise from approximations of the Ni3p peak fitting.

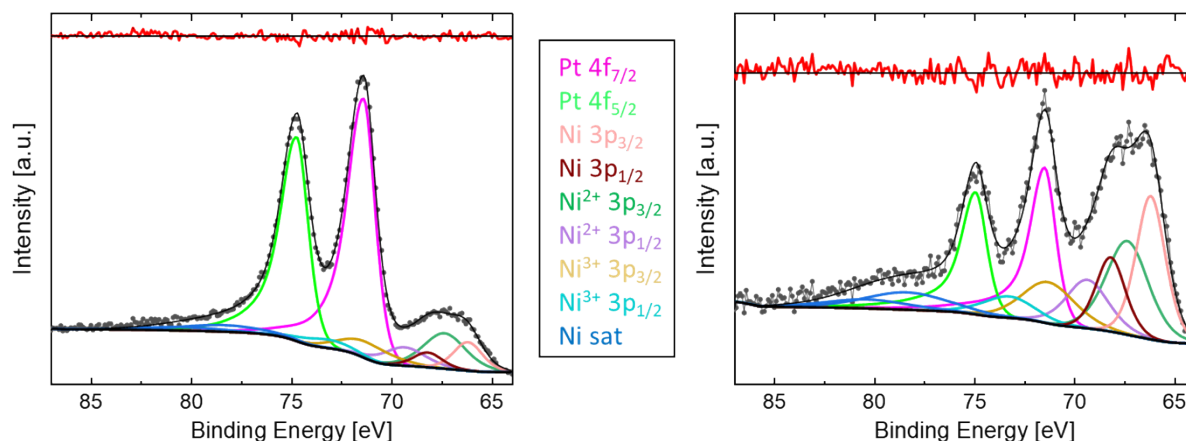


Fig. S23 Peak fitting of XPS data for LNO (without post deposition annealing) exposed to PtO₂ for 24 hrs after 78 and 182 seconds of Ar⁺ sputtering.

High-resolution XPS spectra of La3d (830-880 eV) have been measured for all samples in the current paper and an example is shown in Fig. S24. These spectra are challenging to resolve due to the multiplet splitting of La compound, and in case of LaNiO₃ it is even more challenging to resolve them due to strong overlap with Ni2p. Previous attempts of resolving La3d and Ni2p peaks in LaNiO₃ have been documented in literature [6] and ten component peaks had to be included in the analysis to arrive on a decent fit. This number is expected to be even higher for LNO films after reaction with PtO₂(g) and RhO₂(g), which would further complicate the deconvolution of these peaks. The Ni2p peaks would probably also have several components as we expect both Ni²⁺ and Ni³⁺ in these samples. Quantifying the PGM:La (PGM = Pt, Rh) ratio would likely not make sensible numbers from the data collected for the present study due to the strong La3d and Ni2p peak overlap.

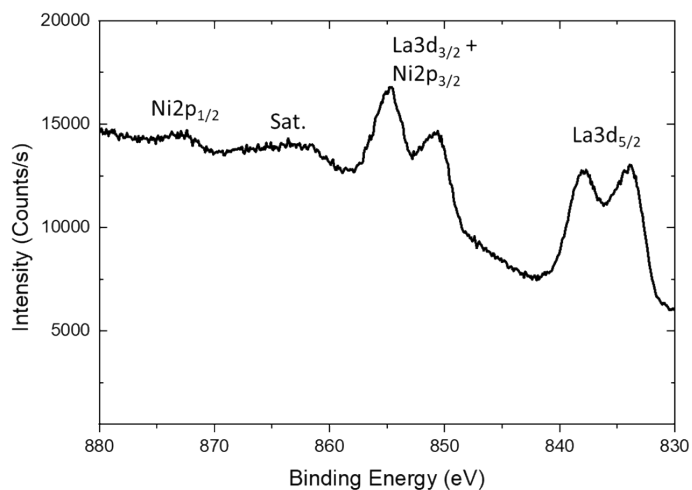


Fig. S24 XPS narrow scan (830-880 eV) showing La3d and Ni2p peaks of LNO thin film sample (without post annealing) after exposure to $\text{PtO}_2(\text{g})$ for 24 hrs.

Section S5. Supplementary figures to results section 3.4 and fitting of XPS data

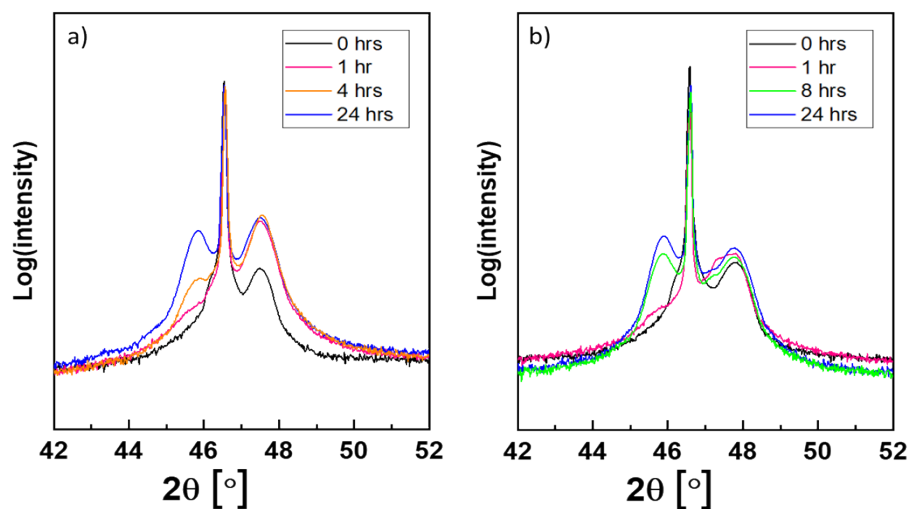


Fig. S25 Powder X-ray diffractograms of LNO films on STO substrates after joint exposure to $\text{PtO}_2(\text{g})$ and $\text{RhO}_2(\text{g})$ with various exposure times for a) samples of batch 1 with thickness of 88.2 nm and b) samples of batch 2 with 45.3 nm. The diffractogram is zoomed in around the (200) peak of STO and pseudo cubic (200) peak of LNO.

An example of an XPS survey spectrum after joint exposure to $\text{PtO}_2(\text{g})$ and $\text{RhO}_2(\text{g})$ is shown in Fig. S26 below.

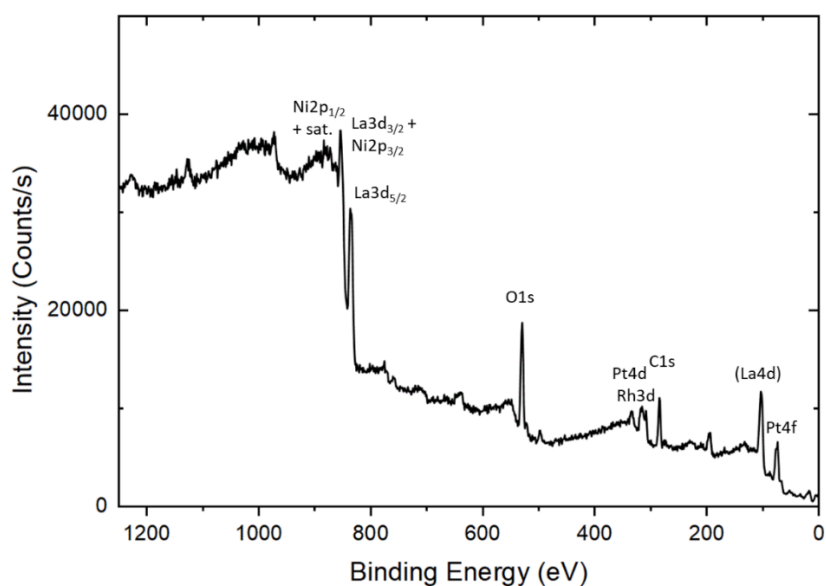


Fig. S26 XPS survey spectrum of LNO (Batch 1 without post annealing) after exposure to $\text{PtO}_2(\text{g})$ and $\text{RhO}_2(\text{g})$ for 4 hrs with the most pronounced peaks identified.

XPS fitting of surface of LNO thin films after joint exposure to $\text{PtO}_2(\text{g})$ and $\text{RhO}_2(\text{g})$:

Narrow scans of Pt4d and Rh3d for LNO sample from batch 2 exposed for 1 hr and 24 hrs (Fig. S27 and Fig. S28) were fitted with one doublet of Pt4d peaks with SOS fixed to 17.00 ± 0.2 eV and one doublet of Rh3d peaks with SOS fixed to 4.71 ± 0.2 eV. For the sample exposed for 24 hrs, extra peaks are assumed to be satellite peaks. The height ratio between $\text{Rh}3\text{d}_{3/2}$ and $\text{Rh}3\text{d}_{5/2}$ and between $\text{Pt}4\text{d}_{5/2}$ and $\text{Rh}3\text{d}_{5/2}$ were fixed to the theoretical values of 0.67. The FWHM of $\text{Pt}4\text{d}_{5/2}$ and $\text{Rh}3\text{d}_{5/2}$ were fixed to be the same as $\text{Pt}4\text{d}_{3/2}$ and $\text{Rh}3\text{d}_{3/2}$ and let to refine. The L-G mix of rhodium and platinum peaks were fixed to 80 %. The asymmetric parameters were fixed to the values found for the reference samples. These are only approximations, but due to the overlap of platinum and rhodium they did not give any meaningful values when let to refine. For the sample exposed for 1 hrs, BE of $\text{Pt}4\text{d}_{5/2}$ ended at 315.8 eV and the BE of $\text{Rh}3\text{d}_{5/2}$ ended at 308.6 eV. For the sample exposed for 24 hrs, BE of $\text{Pt}4\text{d}_{5/2}$ ended at 317.1 eV and the BE of $\text{Rh}3\text{d}_{5/2}$ ended at 308.8 eV.

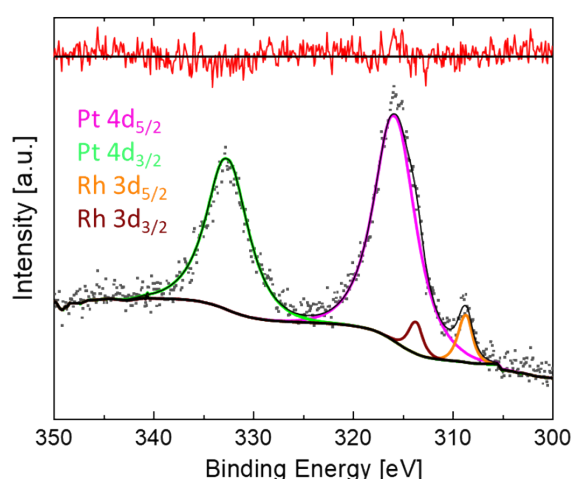


Fig. S27 Peak fitting of XPS data from LNO sample from batch 2 exposed for 1 hr (B2_1hr) with peaks of Pt4d and Rh3d.

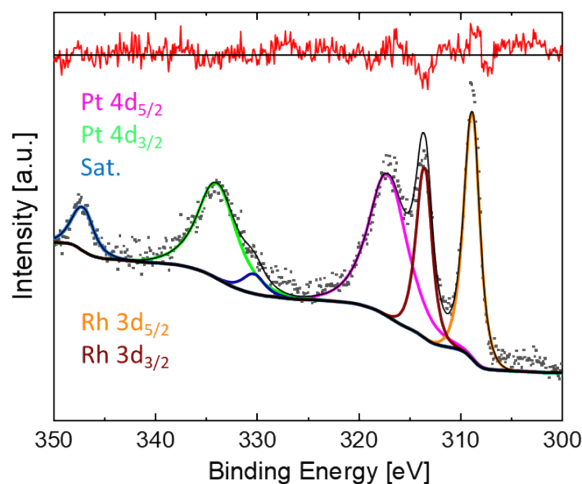


Fig. S28 Peak fitting of XPS data from LNO sample from batch 2 exposed for 24 hrs (B2_24hrs) with peaks of Pt4d and Rh3d.

XPS fitting of Pt4f and Ni3p peaks for LNO (without post deposition annealing) exposed to PtO₂ and RhO₂ for 24 hrs, as shown in Fig. S29, included a doublet of Pt4f with SOS = 3.3 ± 0.2 eV, height ratio of Pt4f_{7/2} to Pt4f_{5/2} = 0.75, L/G-mix of 50 %, FWHM refined to 2.2 eV, while the Ni3p peaks were fitted similar to as shown in Fig. S19a) (except that the height of the satellite/shakup peak was fixed to the same ratio it had in relation to the Ni²⁺ peak in Fig. S19a since it now overlapped with Pt4f_{5/2} and all L/G-mix values were fixed to 50%). The BE of Pt4f_{7/2} was fitted to 72.6 eV.

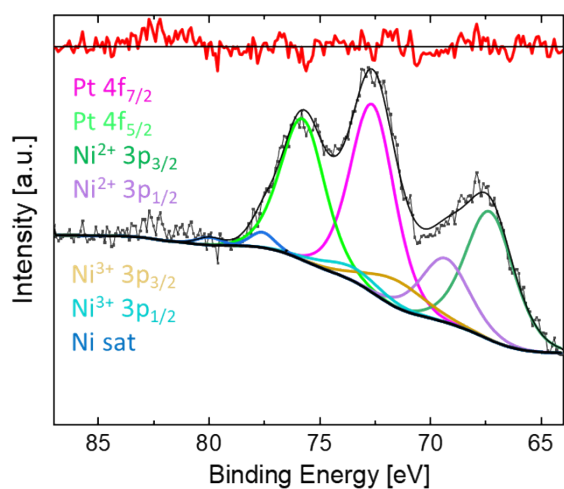
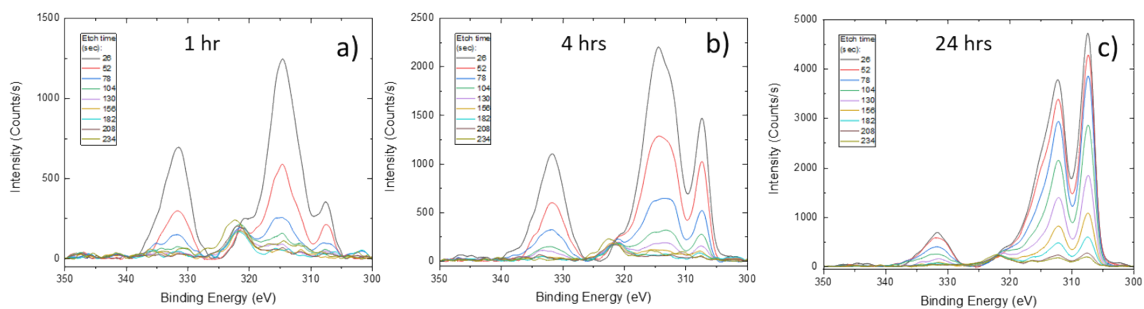


Fig. S29 Peak fitting of XPS data from LNO sample from batch 1 exposed for 24 hrs (B1_24hrs) with peaks of Pt4f and Ni3p peaks.

Batch 1



Batch 2

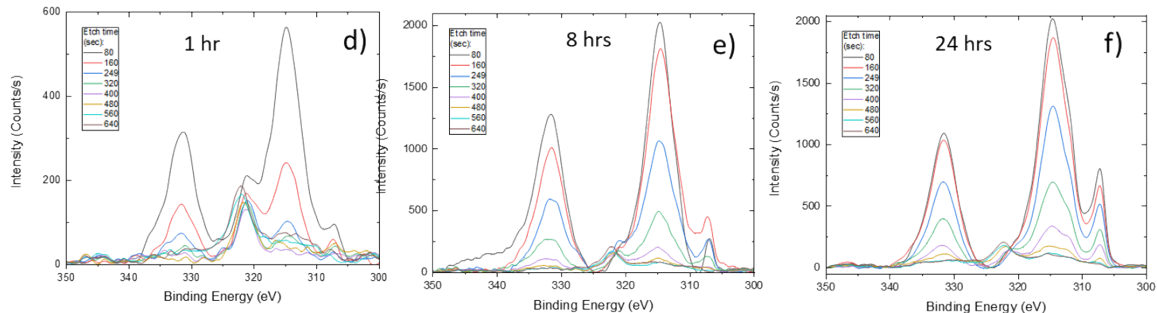


Fig. S30 XPS narrow scans of Pt4d and Rh3d (300-350 eV) at the different sputtering levels after sequential sputtering with Ar⁺ and measuring with XPS through the depth of the film for LNO (without post deposition annealing) after joint PtO₂ and RhO₂ exposure for 1, 4 (B1), 8 (B2) and 24 hrs. The background was removed and the spectrum was smoothed with a gaussian function (FWHM ~ 0.5 eV) for more easy visualization of data.

References

- [1] J. Landoulsi, M.J. Genet, S. Fleith, Y. Touré, I. Liascukiene, C. Méthivier, P.G. Rouxhet, Organic adlayer on inorganic materials: XPS analysis selectivity to cope with adventitious contamination, *Appl. Surf. Sci.* 383 (2016) 71–83. <https://doi.org/10.1016/j.apsusc.2016.04.147>.
- [2] L. Qiao, X. Bi, Direct observation of Ni³⁺ and Ni²⁺ in correlated LaNiO_{3-δ} films, *Europhys. Lett.* 93 (2011) 57002. <https://doi.org/10.1209/0295-5075/93/57002>.
- [3] G.H. Major, V. Fernandez, N. Fairley, E.F. Smith, M.R. Linford, Guide to XPS data analysis: Applying appropriate constraints to synthetic peaks in XPS peak fitting, *J. Vac. Sci. Technol. A* 40 (2022) 063201. <https://doi.org/10.1116/6.0001975>.
- [4] A.C. Miller, G.W. Simmons, Nickel by XPS, *Surf. Sci. Spectra* 1 (1992) 312–317. <https://doi.org/10.1116/1.1247658>.
- [5] M. Golarikhani, Q. Lei, R.U. Chandrasena, L. Kasaei, H. Park, J. Bai, P. Orgiani, J. Ciston, G.E. Sterbinsky, D.A. Arena, P. Shafer, E. Arenholz, B.A. Davidson, A.J. Millis, A.X. Gray, X.X. Xi, Nature of the metal-insulator transition in few-unit-cell-thick LaNiO₃ films, *Nat. Commun.* 9 (2018) 2206. <https://doi.org/10.1038/s41467-018-04546-5>.
- [6] S. Mickevičius, S. Grebinskij, V. Bondarenka, B. Vengalis, K. Šliužienė, B.A. Orlowski, V. Osinniy, W. Drube, Investigation of epitaxial LaNiO_{3-x} thin films by high-energy XPS, *J. Alloys Compd.* 423 (2006) 107–111. <https://doi.org/10.1016/j.jallcom.2005.12.038>.